

Evaluation of Dynamic Stall Models with UH-60A Airloads Flight Test Data

Khanh Nguyen
NASA Ames Research Center
Moffett Field, California

Wayne Johnson
Johnson Aeronautics
Palo Alto, California

Abstract

This paper presents an evaluation study of the five dynamic stall models in the rotorcraft comprehensive analysis CAMRAD II. The five models are the Johnson, Boeing, Leishman-Beddoes, ONERA Edlin, and ONERA BH models. Oscillating airfoil results show that all five models can compute the lift stall reasonably well, while the Johnson, Leishman-Beddoes, and ONERA BH models can compute the stall peaks in the pitching moment fairly accurately. In the rotor environment, all stall models predict the stall locations fairly well, but all are unable to compute the right magnitudes of the pitching moment peaks. Proper wake modeling can be crucial in the calculation of the stall events. Small changes in collective pitch and in blade twist distribution do not significantly affect the stall calculation.

Introduction

Accurate prediction of blade stall is crucial in the design of helicopters and the sizing of the rotor structural components. This problem has remained one of the major challenges of the rotorcraft aeromechanics community. Stall limits the rotor structural envelope, in particular, the helicopter maximum speed and the rotor loading capabilities. At the stall boundary, the large blade pitching moment induced by stall can cause stall flutter and excessive loading, leading to fatigue of structural components. In addition, stall increases the rotor shaft torque, causes excessive vibration, and adversely affects the aircraft handling qualities. Efficient rotor design technology requires improved understanding and a reliable prediction of rotor stall.

Classical treatments of rotor stall indicate that stall typically occurs near the retreating blade tip. In forward flight, a blade encounters a time-varying dynamic pressure due to the combination of the blade rotation and the rotor translational speed. Thus, the dynamic pressure is greater on the ad-

vancing side than the retreating side. For roll moment balance, the blade operates at angles of attack that are low on the advancing side and high on the retreating side. At high blade loading, the local blade section angle of attack can become large enough to initiate stall.

Operating in an unsteady environment, the most severe type of stall encountered by a rotor blade is dynamic stall. In forward flight, the blade experiences time-varying dynamic pressure and angle of attack arising from blade pitch inputs, elastic responses, and non-uniform rotor inflow. If supercritical flow develops under dynamic conditions, then dynamic stall is initiated by leading edge or shock-induced separation. Even though understandings about the development of supercritical flow in the rotor environment are quite limited, flow visualization results of oscillating airfoil tests at low Mach number suggest that supercritical flow is associated with the bursting of the separation bubble as the bubble encounters the large adverse pressure gradient near the blade leading edge [1]. Dynamic stall is characterized by the shedding of strong vortices from the leading edge region. The leading edge vortex produces a large pressure wave moving aft on the airfoil upper surface and creating abrupt changes in the flow field. The pressure wave also contributes to large lift and moment overshoots in excess of static values and prolongs flow separation, both causing significant nonlinear hysteresis in the airfoil behavior.

The other type of stall typically observed in two-dimensional wind tunnel tests involves trailing edge separation. The phenomenon of trailing edge separation is associated with either static or dynamic conditions. Separation starts from the airfoil trailing edge, and with increasing angle of attack, the separation point progresses towards the leading edge region. Trailing edge separation contributes to nonlinear behavior, such as hysteresis, in lift, drag and pitching moment due to the loss in circulation. In contrast to dynamic stall that is characterized by abrupt changes in airfoil behavior, trailing edge stall progresses at a moderate rate.

A recent investigation of blade pressure data from the UH-60A Airloads Program [2] has helped improve understanding about rotor stall behavior. Test results reveal that stall is not confined solely to the retreating side but rather spreads to the first quadrant of the rotor disk. Since stall is strongly coupled with the blade dynamics, especially the torsion mode, this coupling manifests in a stall cycle that begins in the fourth quadrant of the rotor disk and continues up to the first quadrant in two cycles (three stall peaks). The stall cycle has a frequency closely matched with the blade torsion frequency. Note that this stall event is distinct from another stall pattern, identified from flight test data, that occurs in the inboard region of the third quadrant and is attributed to fuselage upwash. Flight test data also indicate that rotor stall exhibits behaviors similar to that observed in airfoil oscillating tests where the shedding of the strong leading edge vortex dominates the flow pattern. After shedding, the leading edge vortex traverses over the blade upper surface, causes a sharp nose down pitching moment (moment stall) and a lift build up, which are followed by an abrupt loss in lift (lift stall) and a subsequent trailing edge flow separation. The flow over the airfoil may or may not fully reattach before the next stall cycle.

Stall data from the UH-60A Airloads Program is used in this paper to evaluate the different dynamic stall models. Most of the dynamic stall models currently used in rotorcraft analyses are semi-empirical, synthesized from oscillating airfoil test data. As suggested by the flight test results, the strong correlation between the development of the stall cycles and the blade torsion dynamics suggests any meaningful analyses of rotor stall must include aeroelastic effects. Accurate computation of the vehicle trim and rotor inflow must also be included. The availability of five dynamic stall models in a new version of CAMRAD II, a comprehensive rotorcraft analysis, facilitates the evaluation study. These five dynamic stall models are from Boeing [3], Johnson [4], Leishman-Beddoes [5], and ONERA Edlin (for Linear Differential Equations) [6], and ONERA BH (for Hopf Bifurcation) [7].

First, CAMRAD II results using all five models are compared with the oscillating airfoil data from both the NACA 0012 and the SC-1095 airfoils to verify the proper modeling of the isolated stall models. Then, the rotorcraft analyses with the five stall models are compared with the UH-60A airload data for a steady-level flight condition with significant

rotor stall. The study aims to determine whether the current stall models are adequate for rotorcraft analyses and which models better capture the rotor stall. The effects of the rotor operating conditions, rotor wake modeling, and blade twist on the stall behavior are also investigated.

CAMRAD II Analysis

This section aims to provide a brief overview of the CAMRAD II analysis and of the stall models used in the paper. Reference 8 provides further details on the analysis, and Ref. 9 on the dynamic stall models as implemented in CAMRAD II.

CAMRAD II is an analysis of rotorcraft aeromechanics that includes multi-body dynamics, nonlinear finite elements, and rotorcraft aerodynamics. Multibody mechanics allows modeling of large rigid body motion with exact kinematics. The finite element model provides an elastic blade model that includes beam bendings, torsion, and extension. The blade elastic model is based on beam theory with small strain and moderate deflections. The analysis computes the blade airloads with lifting-line theory, using two-dimensional airfoil characteristics and vortex wake for rotor inflow. The aerodynamic model has corrections for yawed and swept flows. The options for inflow models are uniform inflow, prescribed wake, and free wake with either one or two tip vortices (dual peak model).

The five dynamic stall models available in CAMRAD II are the Johnson model, the Boeing model, the Leishman-Beddoes model, the ONERA Edlin model, and the ONERA Hopf Bifurcation (BH) model. As implemented, all the stall models compute components of the stalled loads from the values within the static airfoil tables based on a stall delayed angle of attack. The stall delayed angle of attack can include unsteady attached flow effects.

Compared to the other three stall models, both the Johnson and the Boeing models are relatively simple models with the delayed angle of attack driven by the pitch rate. The Johnson model uses a delayed angle of attack proportional to the pitch rate and three delay parameters, one each for lift, drag, and pitching moment. The leading edge vortex is modeled with two distinct lift and moment increments, initiated after the delayed angle of attack reaches a prescribed dynamic stall angle.

The Boeing model uses a delayed angle of attack model that is proportional to the square root of the pitch rate and three delay parameters, one each for lift, drag, and pitching moment. The Boeing model does not include separate lift and pitching moment increments due to the leading edge vortex.

In the Leishman-Beddoes dynamic stall model, the delayed angle of attack is governed by two distinct processes, each of which is modeled with a first order linear dynamic model. The first process is associated with the airfoil pressure response and is driven by the attached flow lift. The second deals with the boundary layer response and is driven by the trailing edge separation distance (measured from the trailing edge), obtained from the Kirchhoff model. As implemented in CAMRAD II, the delayed angle of attack allows the computation of the nonlinear lift, drag, and pitching moment without the leading edge vortex effects, directly from the static airfoil tables. Also, the criterion for initiating the shedding of the leading edge vortex is the delayed trailing edge separation distance exceeds 30 percent of the airfoil chord. Once shed, the leading edge vortex is modeled by another first order linear dynamic model. The Leishman-Beddoes dynamic stall model requires eight parameters, four of which depend on the airfoil characteristics.

The ONERA Edlin model employs three second-order linear dynamic systems for the leading vortex load increments, driven by the differences between the linear and nonlinear lift, drag, and pitching moment. The delayed angle of attack is computed based on a first-order linear dynamic model, and the model requires 22 parameters.

The three second-order dynamic systems for the leading vortex load increments in the ONERA BH model are nonlinear and are driven by the time derivatives of the angle of attack. The coefficients used in the equations require 18 parameters and have values that depend on whether the flow is separating or reattaching, resulting in two distinct dynamic processes. The separating flow process is governed by a Van-der-Pol-Duffing type equation that yields a chaotic response (non-periodic), while a damped oscillator is used for the reattaching flow. As implemented in CAMRAD II, the switching condition (or Hopf condition) occurs when the trailing edge separation distance crosses a prescribed critical value. For the delayed angle of attack calculation, the model employs a scheme

adapted from the Leishman-Beddoes model. The ONERA BH model requires 18 parameters.

Validation of Stall Models with Airfoil Data

The oscillating airfoil data obtained by McAlister et. al [10] is used to evaluate the dynamic stall models in CAMRAD II under the prescribed angle of attack conditions. The test program, performed in the U.S. Army 7- by 10-Foot Wind Tunnel, includes eight test models, each with a two-foot chord and different airfoil sections. Test results include both static and oscillatory airfoil data at free stream Mach number up to 0.3. The integrated lift and pitching moment are obtained from the 26 pressure transducers distributed over the upper and lower surface of the models.

Figure 1 shows the comparison of the computed lift with test data for the oscillating NACA-0012 airfoil (Frame 10022 of Ref. 10). The test conditions are 0.301 Mach number, 0.098 reduced frequency; the mean and oscillatory pitch are 11.84 and 9.87 deg, respectively. CAMRAD II results are obtained by direct numerical integration of the dynamic stall governing equations. Figure 1(a) shows the Johnson and Boeing results, and Fig. 1(b) the Leishman-Beddoes, ONERA Edlin, and ONERA BH results. The Boeing model captures the lift hysteresis well in both the upstroke and the downstroke. The Johnson model performs equally well in the upstroke, slightly overpredicts the lift overshoot in the 17–20 deg angle of attack range. In the downstroke, the Johnson model overpredicts the lift by an almost uniform amount over the complete range of angle of attack. Referring to Fig. 1(b), the Leishman-Beddoes and both ONERA models capture the lift behavior quite well in the upstroke. The ONERA Edlin model prolongs the stall delay, yielding a larger lift overshoot than test data. In the downstroke, the Leishman-Beddoes model overpredicts the lift, the ONERA Edlin underpredicts it, while the ONERA BH model has a lift behavior that oscillates about the test data.

The pitching moment comparisons of the NACA 0012 are shown in Fig. 2. The Johnson model captures the moment overshoot magnitude but misses its phase by 2.5 deg; the Boeing model seems to capture the right phase but underpredicts the magnitude by roughly two-third. Both models poorly predict the moment reattachment process. In Fig. 2(b), the ONERA BH model captures both

magnitude and phase of the moment overshoot quite well, while Leishman-Beddoes model has the right phase and a magnitude 25 percent higher than test data. In the downstroke, the Leishman-Beddoes model performs reasonably well, showing a reattachment rate slower than test data. The oscillatory behavior of the ONERA BH result suggests a peculiar second moment overshoot, absent in the test data. The ONERA Edlin model severely underpredicts the moment overshoot.

Before proceeding to the oscillating SC-1095 results, it is worth noting that all five stall models are semi-empirical, and thus the computed results are highly dependent on the parameters used in each model. Since the parameters available in CAMRAD II at the time of this study are limited to those developed for the NACA 0012 airfoil, good correlation results are expected for most of these models as shown earlier. However, good correlation results when the same parameters are used to analyze the stall behavior of airfoils other than the NACA 0012 are expected.

The results for the oscillating SC-1095 airfoil are shown in Figs. 3 and 4. The test data are obtained from Frame 37305 of Ref. 10, corresponding to the 0.3 Mach number, 0.10 reduced frequency; 11.86 deg mean pitch with oscillatory component of 7.9 deg. In the upstroke, the Boeing model captures the lift behavior well but underpredicts the lift in the downstroke (Fig. 3a). The Johnson model overpredicts the lift overshoot but captures the downstroke behavior well. Both the Leishman-Beddoes and the ONERA BH models slightly underpredict the lift overshoot magnitude but perform reasonably well in the downstroke (Fig. 3b). The ONERA Edlin model captures lift behavior in the upstroke well, but underpredicts the downstroke values as in the NACA 0012 results.

Figure 4 shows the pitching moment results for the SC-1095. As in the NACA 0012 results, the Boeing model underpredicts the moment overshoot, while the Johnson model is again capable of capturing the right magnitude but misses the phase. The Leishman-Beddoes model captures well both the magnitude and phase of the moment overshoot as well as the reattachment behavior. The ONERA BH results also show good correlation with test data but slightly underpredicts the overshoot value. As in the NACA 0012 results, the ONERA Edlin model underpredicts the moment overshoot by a significant amount.

Note that the good correlation results of the Leishman-Beddoes and ONERA BH shown in Figs. 3 and 4 are due in part to the fact that the C_{LMAX} value, critical to these models, are obtained from the static data of the same test program at 0.3 Mach number (Frame 35021 of Ref. 10). The C_{LMAX} value is critical because it is used to dictate the condition for initiating dynamic stall process in both models. An attempt to use the value from the airfoil table commonly used in the UH-60A analyses [11] lead to poor correlation results for these two stall models.

Validation of Stall Models with Flight Test Data

The flight test data from the UH-60A Airloads Program [12] are used to evaluate the capability of CAMRAD II analysis with these dynamic stall models to compute blade airloads under stall conditions. The aircraft has a four-bladed fully-articulated rotor with 20 deg swept tip blades. One of the blades was fully instrumented with 221 pressure transducers for airloads measurements at nine radial stations. The integrated pressure data yield the blade section normal force (normal to the chord line) and aerodynamic pitching moment. To obtain high rotor loading, the UH-60A Airloads aircraft was flown at normal gross weight but at high altitude for reduced density.

The CAMRAD II model of the UH-60A rotor is an adaptation of a CAMRAD/JA model [13] and subsequently updated as described in Ref. 14. The updates include a reduced blade flapwise and chordwise stiffnesses that reflect the absence of the nickel abrasion strip in the outboard region of the pressure-instrumented blade. Another update include the effects of the chordwise c.g. shift due to instrumentation wiring. The blade pre-pitch over the SC-1095R8 segment is reduced by 1 deg, consistent with description of the airfoil chord line. The airfoil tables of the SC-1095 and the SC-1095R8 are adapted from those reported in Ref. 11. Finally, the updated value of the pitch-link stiffness, based on the recently completed control stiffness measurement at NASA Ames [14], is included. In particular, a single spring is used to model both the pitch-link stiffness and the flexibility of the control system in the non-rotating frame, yielding a blade torsion frequency of 4.1 per rev at the nominal rpm of 258.

In order to simplify the analysis, a wind tunnel trim simulation is used. The prescribed variables are the rotor shaft tilt, cyclic flapping angle, and either the aircraft weight coefficient-solidity ratio (C_w/σ) or the collective pitch. Trimming to C_w/σ is desirable but is sometimes unachievable due to the numerical convergent difficulties associated with the impulsive loading of dynamic stall.

The evaluation study uses test data from a steady-level flight, corresponding to a C_w/σ of 0.13 and designated as Counter 9017 in the UH-60A Airloads Program. For this flight condition, the advance ratio is 0.236, the forward shaft tilt is 3 deg, and the lateral and longitudinal cyclic flapping, measured at the blade flapping hinge, are 9 and -7 deg, respectively.

Effects of Stall Models. The evaluation of the different dynamic stall models is carried out with a prescribed collective pitch setting of 15 deg for the Counter 9017 flight. The rotor inflow is calculated with the dual-peak free wake model, and the Leishman-Beddoes attached flow model is used to calculate the attached flow unsteady airloads. Figure 5 shows the lift over the rotor disk for the flight test data and for the CAMRAD II results obtained with the static stall, Johnson, Boeing, Leishman-Beddoes, and ONERA Edlin models. The numerical solutions with the ONERA BH model are divergent, and hence no results are presented. In Fig. 5, the lift is represented by $C_N M^2$ where C_N is the normal force coefficient and M is the Mach number.

In Fig. 5(a), the flight test data shows two stall events in the outboard blade region in the fourth quadrant of the rotor disk. The overall comparisons of the rotor lift distribution between the test data and CAMRAD II results are fair in general. The static stall model produces a single small stall event at the blade tip in the fourth quadrant. The two stall events produced by the Johnson model occur prematurely, as in the two-dimensional cases, and have smaller magnitudes compared to the test data. The Boeing model produces several stall regions, all distributed along the blade span in the 300–360 azimuth range. The Leishman-Beddoes results are virtually identical to the static stall results, both fail to predict any significant stall events. The ONERA Edlin model produces two stall events in the fourth quadrant, the first one appears to occur prematurely compared to test data.

Figure 6 shows the pitching moment distribution. The most prominent feature of the moment data are the two stall peaks in the outboard blade region in the fourth quadrant. The subsequent moderately large pitching moment near the outboard region suggests that the passage of the leading edge vortex has delayed flow reattachment up to the first quadrant. The stall region produced by the static stall model exhibits a phenomena associated with trailing edge stall. As expected, this stall model does not produce the two stall peaks, prominent in the test data and attributed to the leading edge vortex shedding. For this case, the Johnson model performs better in predicting pitching moment than lift. The model produces two stall events at the locations that match with test data but have lower magnitudes. The Boeing model produces several stall events, all of which have lower magnitudes than the two prominent peaks in the test data. As in the lift results, the Leishman-Beddoes results for pitching moment is similar to that of the static stall model. Since this model has been shown in the two-dimensional cases to be particularly sensitive to the airfoil $C_{L,MAX}$, the inability of the Leishman-Beddoes model to produce any significant stall events suggests the airfoil tables need to be assessed. The ONERA Edlin model produces two stall events at the locations matching that with test data but having lower magnitudes.

Effects of Rotor Inflow Models and Collective Pitch. Figure 7 and 8 shows the computed lift and pitching moment distributions using the uniform inflow and dual-peak free wake models. The numerical results are conducted at 16.5 deg collective pitch, using the Leishman-Beddoes dynamic stall model. The prescribed wake results are virtually identical to that for the free wake and are not shown. The comparison clearly indicates the sensitivity of the computed airloads to the wake models for this flight condition. Note that the shaft angle for this flight condition is only 3 deg forward, and thus the wake effects are quite prominent in the rotor inflow. The pitching moment plots shown in Fig. 8 further reinforce the fact that proper wake modeling is important for pitching moment computation.

Comparing the results of Figs. 7(b) and 8(b) at 16.5 deg collective with that of Figs. 5(e) and 6(e) at 15 deg collective shows the effects of increasing collective pitch on the stall computation of the

Leishman-Beddoes model in a rotor environment. The comparisons indicate that the increase in collective pitch does not help improve the calculated results.

Effects of Blade Pre-Twist. One unique feature of the UH-60A rotor is the use of positive twist in the outboard 94 percent of the blade. The effects of eliminating the positive twist region are evaluated analytically using two linear twists: a high twist of -15.7 deg and a low twist of -12.7 deg. Figure 9 shows the twist distributions for these cases. In the analysis, the Leishman-Beddoes dynamic stall model and the dual-peak free wake model are used; the rotor is trimmed to a C_w/σ of 0.13. The results for the high twist are shown in Fig. 10. The low twist rate results are virtually identical to that of the high twist and are not presented. Since the results of Fig. 10 are similar to that of Figs. 7(b) and 8(b), it is concluded that small changes in the blade twist, as considered in this study and within the modeling capabilities of CAMRAD II, do not significantly affect the stall behavior of rotors.

Concluding Remarks

An analytical investigation was conducted to evaluate the capabilities of the five dynamic stall models in the comprehensive analysis CAMRAD II to compute the stall behavior in both the two-dimensional and the highly three-dimensional rotor environment. The five stall models are the Johnson, Boeing, Leishman-Beddoes, ONERA Edlin, and ONERA BH models.

For the two-dimensional cases, all five models compute the stalled lift reasonably well. Both the Boeing and the ONERA Edlin models underpredict the magnitude of the pitching moment peaks during dynamic stall. The Leishman-Beddoes model seems to produce the most reliable results compared to test data but is found to be quite sensitive to the $C_{L_{MAX}}$ values from the airfoil tables.

In the rotor environment, all stall models predict the stall locations fairly well, but all are unable to compute the correct magnitudes of the pitching moment peaks. The ONERA BH model can cause the numerical solutions to diverge. Proper wake modeling can be crucial in the calculation of airloads, in general, and of stall events, in particular. Small changes in collective pitch and in blade twist distribution do not affect the stall calculation significantly as considered in this study.

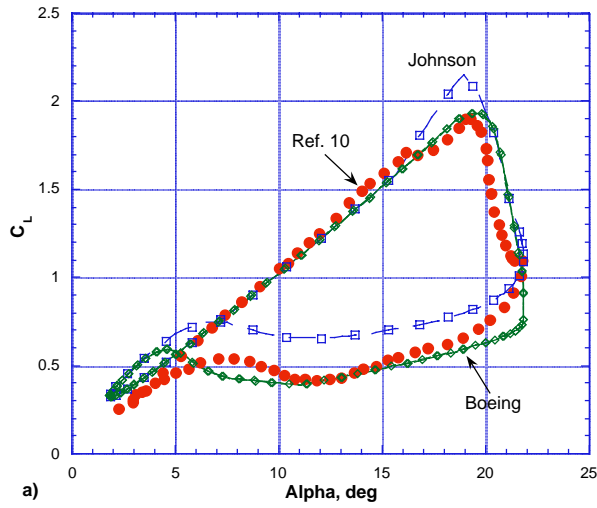
Acknowledgments

The authors would like to thank Mr. Robert Kufeld for the help in setting up the CAMRAD II structural model and in extracting test data from the UH-60A Airloads Program.

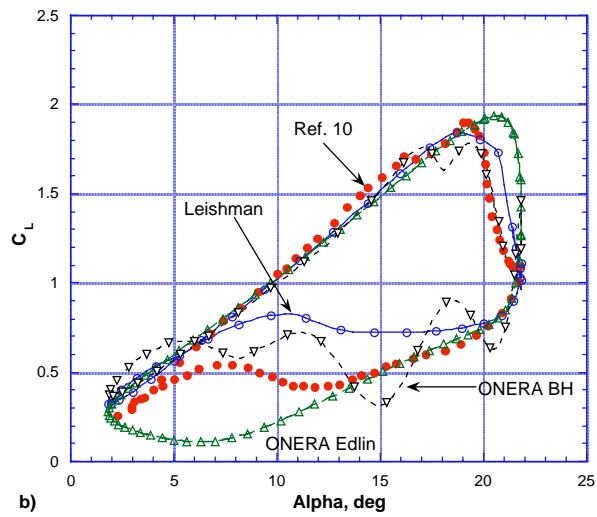
References

1. McCroskey, W. J., Carr, L. W., and McAlister, K. W., "Dynamic Stall Experiments on Oscillating Airfoils," *AIAA Journal*, Vol. 14, No. 1, 1976, pp. 57-63.
2. Bousman, W. G., "A Qualitative Examination of Dynamics Stall from Flight Test Data," Proceedings of the American Helicopter Society 53rd Annual Forum, Virginia Beach, VA, May 1997.
3. Gormont, R. E., "A Mathematical Model of Unsteady Aerodynamics and Radial Flow for Application to Helicopter Rotors," USAAVLABS TR 72-67, May 1973.
4. Johnson, W., "The Response and Airloading of Helicopter Rotor Blades Due to Dynamic Stall," Massachusetts Institute of Technology, ASRL TR 130-1, May 1970.
5. Leishman, J. G. and Beddoes, T. S., "A Semi-Empirical Model for Dynamic Stall," *Journal of the American Helicopter Society*, Vol. 24 (3), Jul 1989.
6. Petot, D., "Differential Equation Modeling of Dynamic Stall," *La Recherche Aeronautique*, No. 1989-5.
7. Truong, V. K., "A 2-D Dynamic Stall Model Based on a Hopf Bifurcation," Proceedings of the 19th European Rotorcraft Forum, Cernobbio, Italy, Sep 1993.
8. Johnson, W., "CAMRAD II, Comprehensive Analytical Model of Rotorcraft Aerodynamics and Dynamics," Johnson Aeronautics, Palo Alto, CA, 1992-1997.
9. Johnson, W., "Rotorcraft Aerodynamics Models for a Comprehensive Analysis," Proceedings of the American Helicopter Society 54th Annual Forum, Washington D. C., May 1998.
10. McAlister, K. W., Pucci, W. J., McCroskey, W. J. and Carr, L. W., "An Experimental Study of Dynamic Stall on Advanced Airfoil Sections; Volume 2: Pressure and Force Data," NASA TM-84245, Sep 1982.
11. Shanley, J. P., "Validation of UH-60A CAMRAD/JA Input Model," SER-701716, Nov 1991.
12. Kufeld, R. M., Balough, D. L., Cross, J. L., Studebaker, K. F., and Jennison, C. D., "Flight Testing of the UH-60A Airloads Aircraft," Proceedings of the American Helicopter Society 50th Annual Forum, Washington D. C., May 1994.
13. Bousman, W. G. and Maier, T. H., "An Investigation of Helicopter Rotor Blade Flap Vibratory Loads," Proceedings of the American Helicopter Society 48th Annual Forum, Washington D. C., Jun 1992.
14. Kufeld, R. M. and Johnson, W., "The Effects of Control System Stiffness Models on the Dynamic Stall Behavior of A Helicopter," Proceedings of the Ameri-

can Helicopter Society 54th Annual Forum, Washing-



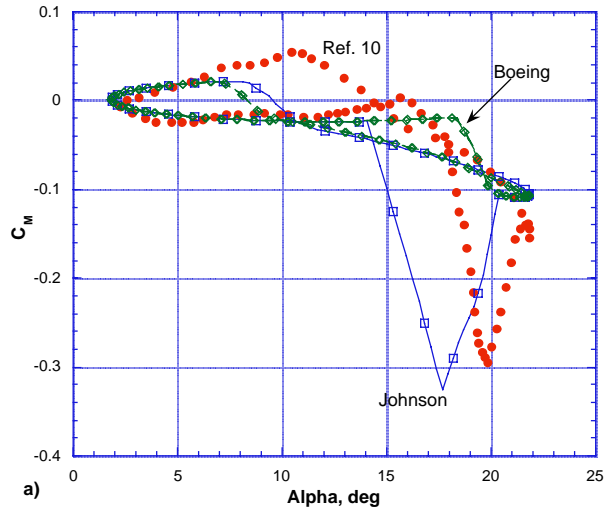
a)



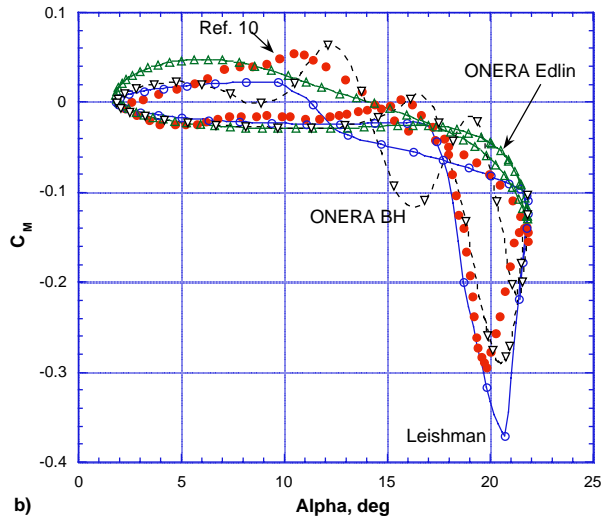
b)

Fig. 1 Comparison of oscillating NACA 0012 lift data with computed results using five dynamic stall models ($\alpha = 11.84 + 9.87 \sin ks$, $k = 0.098$, $M = 0.301$).

ton D. C., May 1998.

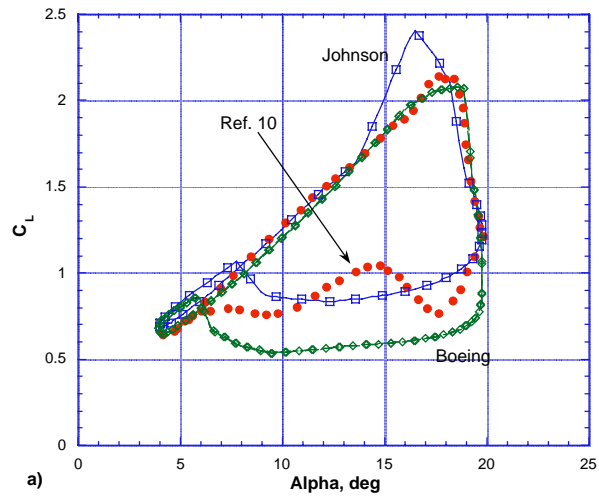


a)

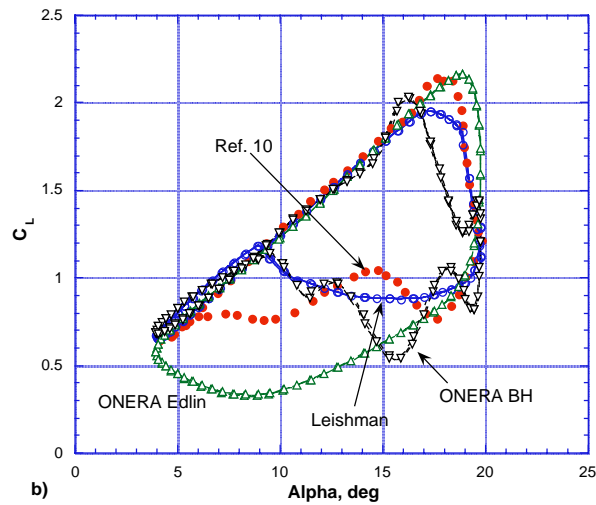


b)

Fig. 2 Comparison of oscillating NACA 0012 pitching moment data with computed results using five dynamic stall models ($\alpha = 11.84 + 9.87 \sin ks$, $k = 0.098$, $M = 0.301$).

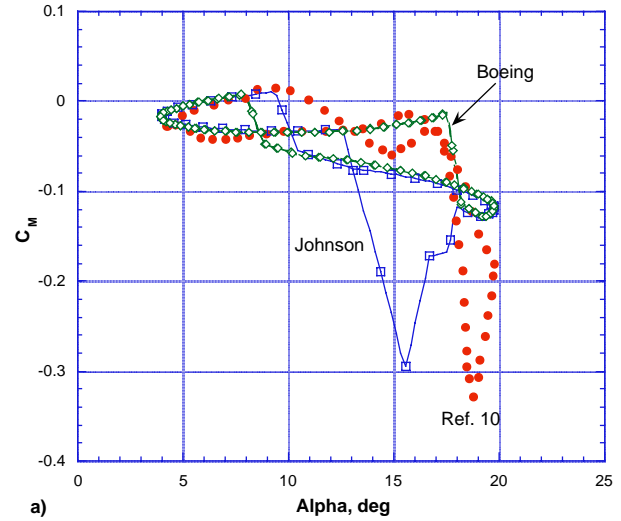


a)

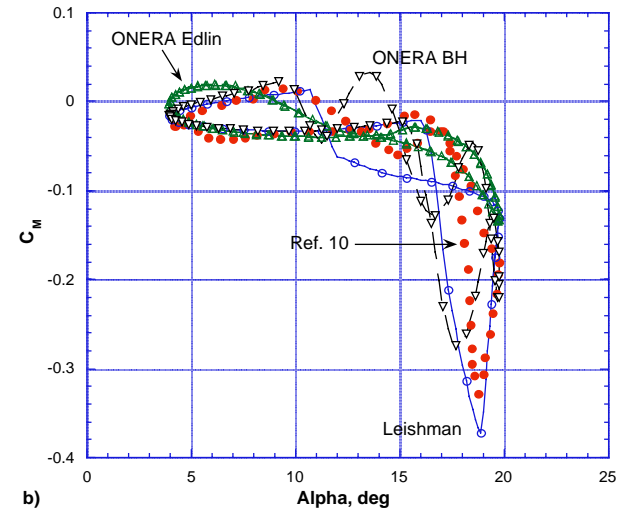


b)

Fig. 3 Comparison of oscillating SC-1095 lift data with computed results using five dynamic stall models ($\alpha = 11.84 + 9.87 \sin ks$, $k = 0.098$, $M = 0.301$).



a)



b)

Fig. 4 Comparison of oscillating SC-1095 pitching moment data with computed results using five dynamic stall models ($\alpha = 11.84 + 9.87 \sin ks$, $k = 0.098$, $M = 0.301$).

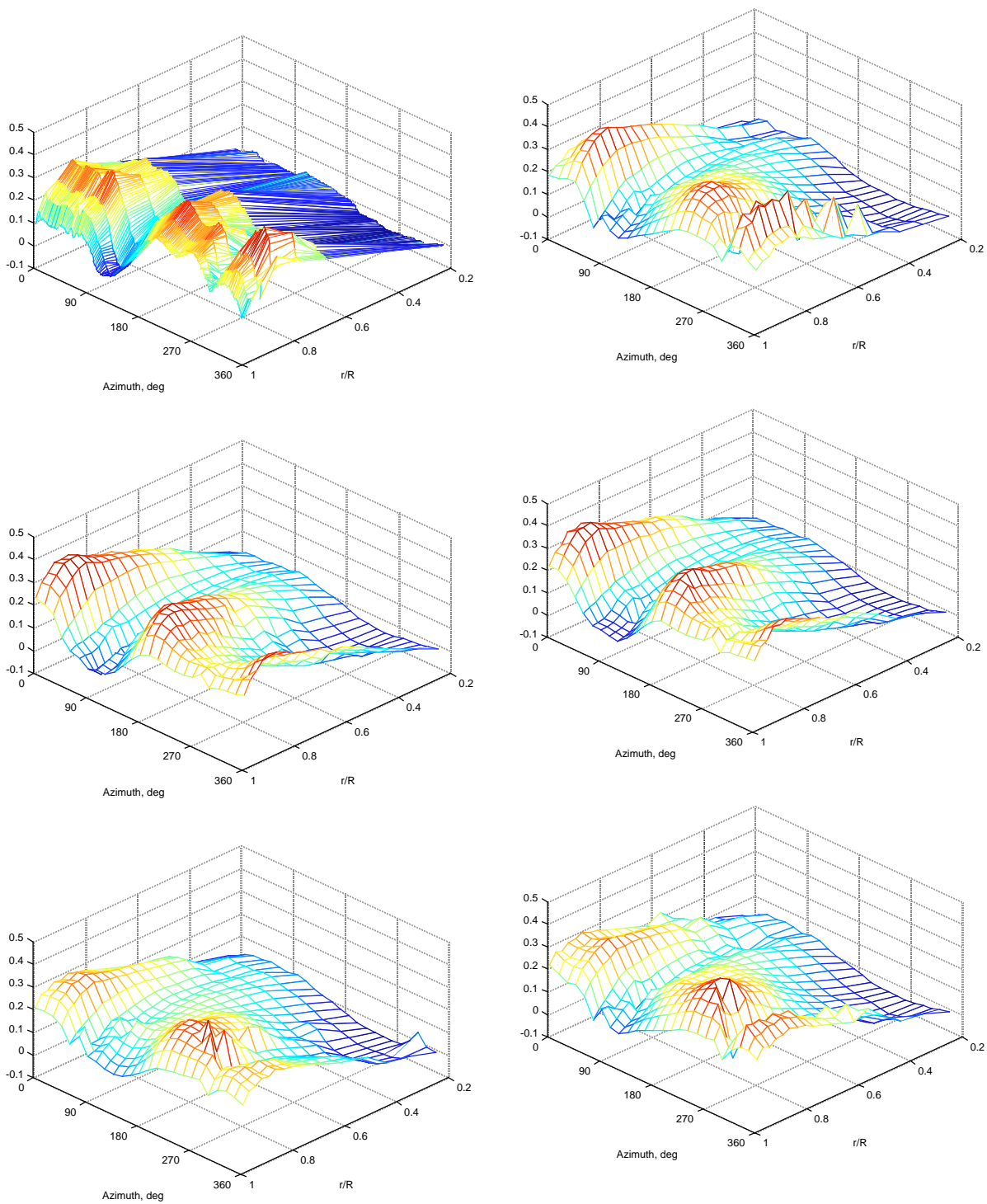


Fig. 5 Comparison of UH-60A lift distribution with computed results using five dynamic stall models, (a) flight test data (Counter 9017, $C_w/\sigma = 0.13$, $\mu = 0.236$.), and analytical results (15 deg collective) (b) static stall model, (c) Johnson model, (d) Boeing model, (e) Leishman-Beddoes model, (f) ONERA Edlin model.

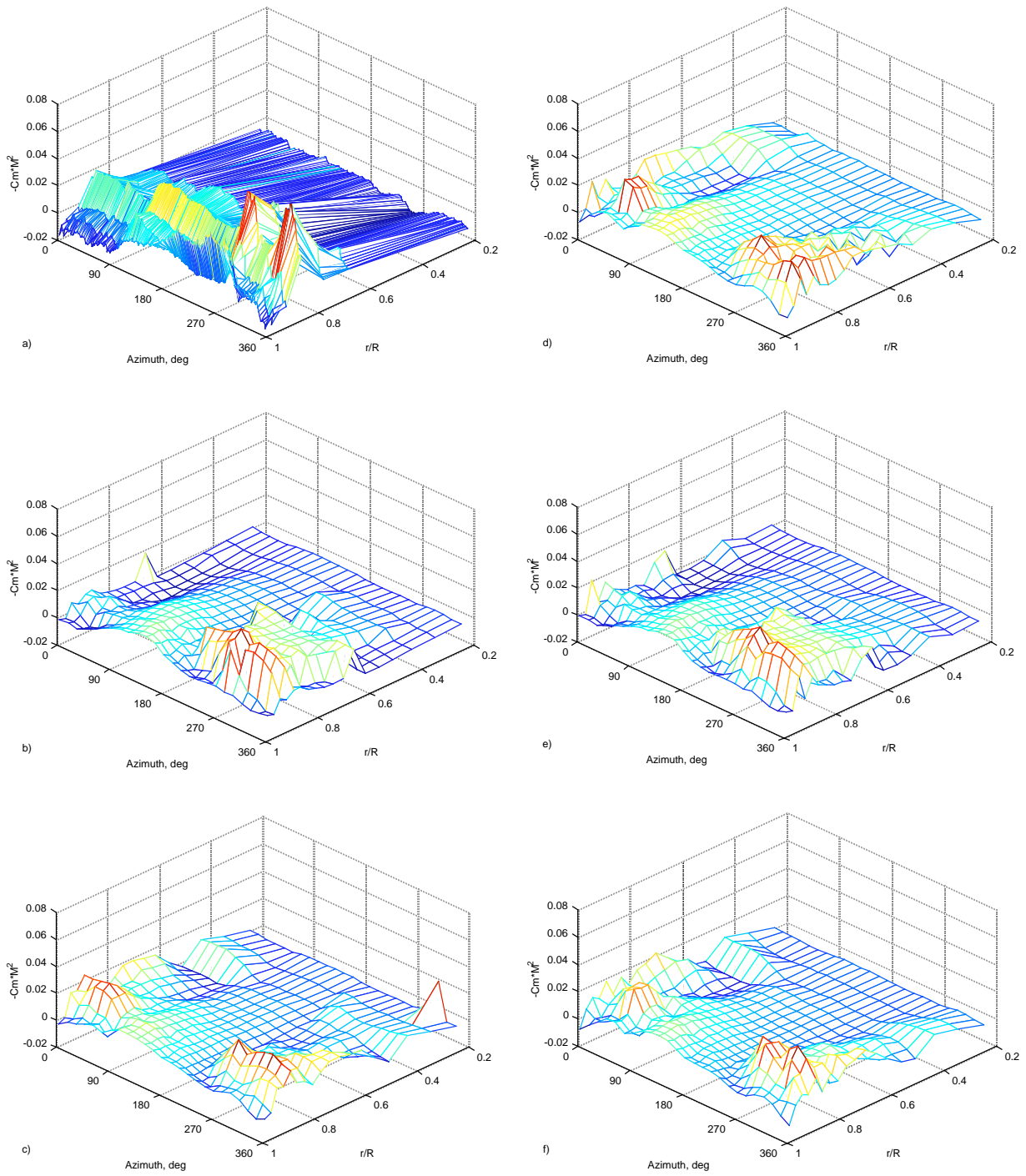


Fig. 6 Comparison of UH-60A pitching moment distribution with computed results using five dynamic stall models, (a) flight test data (Counter 9017, $C_w/\sigma = 0.13$, $\mu = 0.236$), and analytical results (15 deg collective) (b) static stall model, (c) Johnson model, (d) Boeing model, (e) Leishman-Beddoes model, (f) ONERA Edlin model.

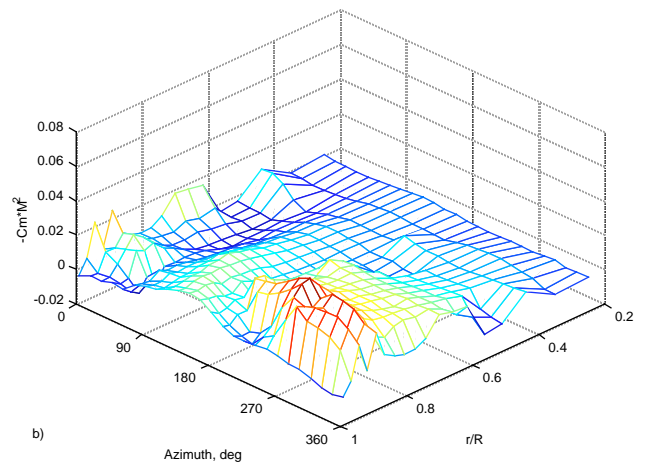
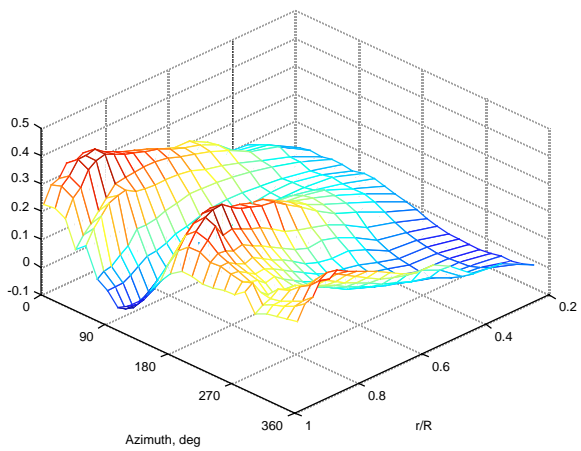
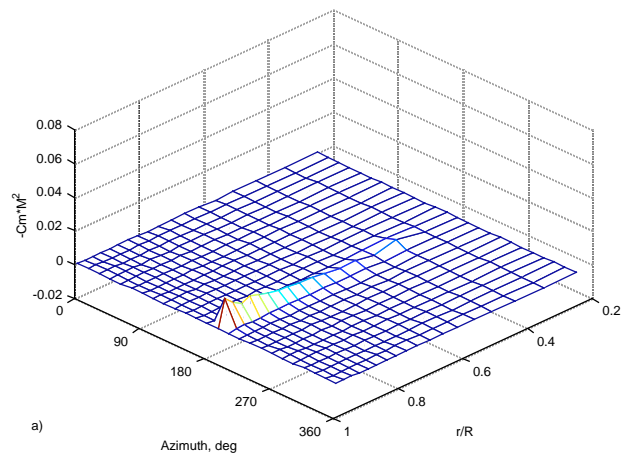
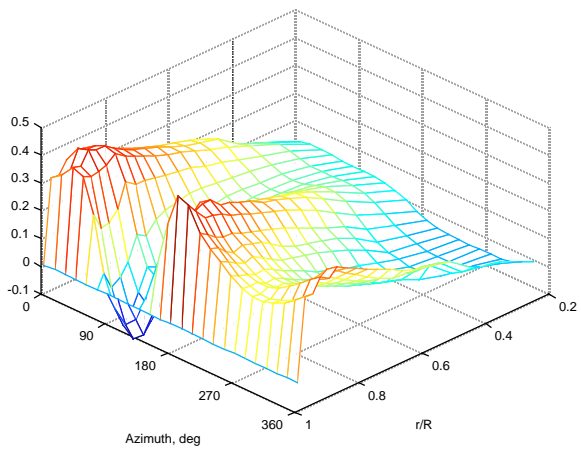


Fig. 7 Effects of inflow modeling on the computed lift on the UH-60A rotor, (a) uniform inflow, (b) dual-peak free wake ($\theta_{75} = 16.5$ deg, $\mu = 0.236$).

Fig. 8 Effects of inflow modeling on the computed pitching moment on the UH-60A rotor, (a) uniform inflow, (b) dual-peak free wake ($\theta_{75} = 16.5$ deg, $\mu = 0.236$).

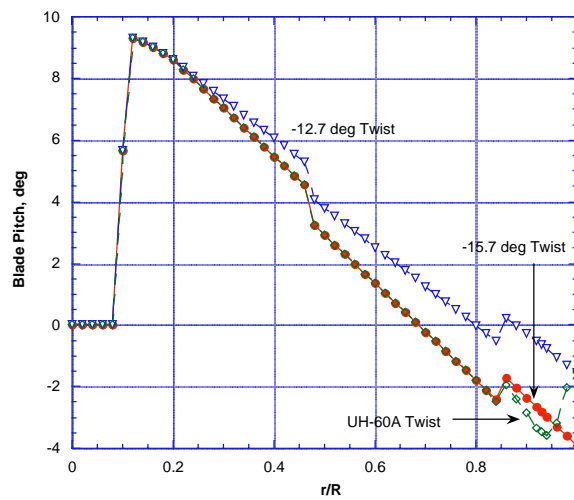


Fig. 9 Twist distributions of UH-60A blade compared to the two linear twist used in the analysis.

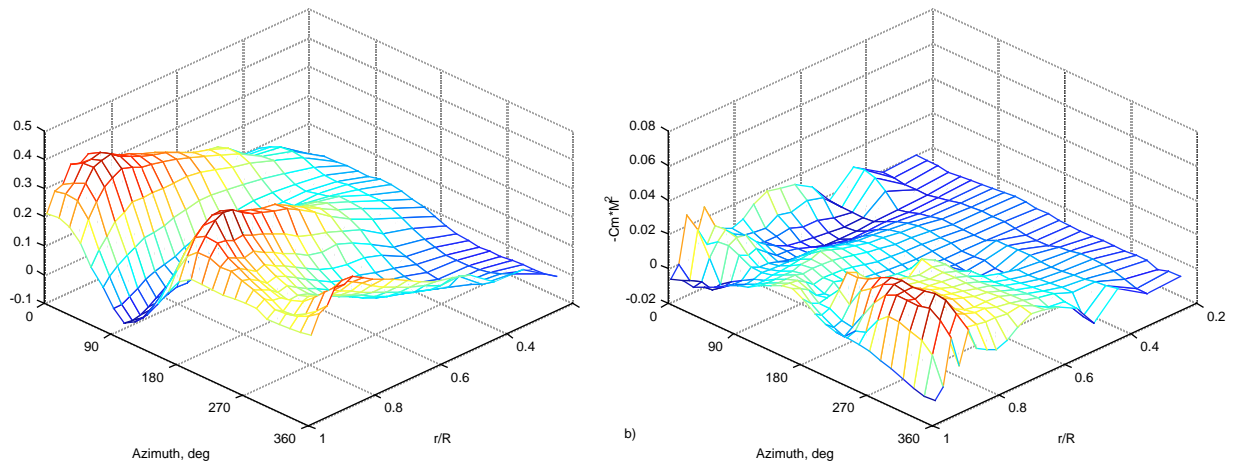


Fig. 10 Computed airloads on the UH-60A with a linear twist of -15.7 deg, (a) lift distribution, (b) pitching moment distribution ($\theta_{75} = 16.5$ deg, $\mu = 0.236$).